

Epi²-Net: Advancing Epidemic Dynamics Forecasting with Physics-Inspired Neural Networks

Rui Sun¹ *, Chenghua Gong¹ *, Tianjun Gu², Yuhao Zheng¹, Jie Ding¹, Juyuan Zhang¹, Liming Pan¹, Linyuan Lü¹ †

¹University of Science and Technology of China

²East China Normal University

{rrsun, gongchenghua}@mail.ustc.edu.cn, {pan_liming, linyuan.lv}@ustc.edu.cn

Abstract

Advancing epidemic dynamics forecasting is vital for targeted interventions and safeguarding public health. Current approaches mainly fall into two categories: mechanism-based and data-driven models. Mechanism-based models are constrained by predefined compartmental structures and oversimplified system assumptions, limiting their ability to model complex real-world dynamics, while data-driven models focus solely on intrinsic data dependencies without physical or epidemiological constraints, risking biased or misleading representations. Although recent studies have attempted to integrate epidemiological knowledge into neural architectures, most of them fail to reconcile explicit physical priors with neural representations. To overcome these obstacles, we introduce Epi²-Net, a **E**pidemic Forecasting Framework built upon **Physics-Inspired Neural Networks**. Specifically, we propose reconceptualizing epidemic transmission from the physical transport perspective, introducing the concept of neural epidemic transport. Further, we present a physic-inspired deep learning framework, and integrate physical constraints with neural modules to model spatio-temporal patterns of epidemic dynamics. Experiments on real-world datasets have demonstrated that Epi²-Net outperforms state-of-the-art methods in epidemic forecasting, providing a promising solution for future epidemic containment. The code is available at: <https://anonymous.4open.science/r/Epi-2-Net-48CE>

1 Introduction

Epidemic transmission poses systemic threats to both human health and societal development. Prolonged SARS-CoV-2 exposure induces not only acute respiratory syndromes but also cardiovascular complications and immune dysfunction (Xie et al. 2022; Al-Aly et al. 2024). Research confirms the COVID-19 pandemic has caused structural economic damage that may persist for decades, with long-term losses surpassing those of regional conflicts (Jordà, Singh, and Taylor 2022). More profound impacts emerge in education, where COVID-19 school disruptions potentially reducing the present value of this cohort’s lifetime earnings by 17 trillion dollars globally (Azevedo et al. 2021). These multidimensional consequences highlight the critical need

for advanced epidemic forecasting models to enable timely health interventions and public policy making.

Epidemic dynamics modeling is currently guided by two primary methodological paradigms: mechanism-based models and data-driven approaches. Mechanism-based models are grounded in epidemiological theory and employ systems of differential equations to characterize disease transmission dynamics. For example, the well-known SIR (Susceptible-Infectious-Recovered) model (Smith, Moore et al. 2004; Cooper, Mondal, and Antonopoulos 2020) and its variants (Heng and Althaus 2020; Poonia et al. 2022) solve partial or ordinary differential equations (PDEs/ODEs) in simulating epidemic transitions between population compartments to generate epidemic predictions. While providing clear epidemiological interpretability, such models incur substantial computational costs when applied at large spatial scales (Bauer, Thorpe, and Brunet 2015) and require careful calibration of key parameters to accurately capture real-time epidemic dynamics. Fundamentally, most mechanism-based models rely on idealized closed-system assumptions (Smith, Moore et al. 2004) and fail to account for the openness and complexity of real-world epidemic spread, including significant factors such as human behavior (Panagopoulos, Nikolentzos, and Vazirgiannis 2021; Hy et al. 2022), social determinants (Nguyen et al. 2023) and geo-spatial interactions (Fan, Varugunda, and Wang 2023), both of which have been proven to significantly alter transmission trajectories.

In contrast, data-driven methods excel at uncovering latent dependencies within historical surveillance data without explicit formulation of spreading mechanisms (Liu et al. 2024). Conventional statistical methods (Mahmud 2020; Kufel 2020) provide a foundational framework for data-driven epidemic forecasting through extracting temporal patterns from time series of daily reported cases. Further, classical machine learning methods have proven effective in capturing the nonlinear temporal dependencies inherent in epidemic dynamics (Wang et al. 2020; Chimmula and Zhang 2020; Galasso, Cao, and Hochberg 2022; Fang et al. 2022), leading to more accurate and robust predictions of outbreaks. With the development of deep learning techniques, recent breakthroughs in neural architectures are revolutionizing data-driven epidemic forecasting. By automatically extracting spatio-temporal signatures from diverse data

*Rui Sun and Chenghua Gong are co-first authors.

†Linyuan Lü is the corresponding author.

streams (case reports, mobility traces, and geographic meta-data), deep learning methods offer transformative potential in modeling epidemic dynamics in real-world scenarios (Panagopoulos, Nikolentzos, and Vazirgiannis 2021; Fan, Varugunda, and Wang 2023; Liu et al. 2024). However, the absence of physical constraints and epidemiological mechanisms in data-driven models may introduce incorrect inductive biases in data-sparse situations, such as during epidemic variations and early outbreaks (Punn, Sonbhadra, and Agarwal 2020). Moreover, data-driven models also suffer from intrinsic interpretability limitations, challenging their adoption for public health policy-making and government intervention measures (Gong et al. 2025; Zhou et al. 2025).

Consequently, the integration of mechanistic principles with data-driven approaches, particularly through physics-inspired deep learning (Raissi, Perdikaris, and Karniadakis 2019), represents a key direction for advanced epidemic forecasting. Although recent studies have attempted to integrate epidemiological knowledge or physical constraints into neural architectures, most of them fail to reconcile explicit physical priors with neural representations (Chen et al. 2018) and exhibit critical limitations as follows:

1) Discrepancy between physical constraints and real-world epidemics. Real-world epidemic dynamics involve complex factors such as human mobility, geographical distance, and lockdown interventions. Currently, mainstream physics-inspired neural methods couple SIR equations with deep learning modules, thereby endowing neural architectures with epidemiological mechanistic (Kosma et al. 2023; Rodríguez et al. 2023). Despite providing certain physical constraints, the SIR model’s inherent closed-system assumption leads to unrealistic simplifications for real-world epidemics (Tian et al. 2024). Such models fail to capture cross-border transmission and spatial attenuation driven by human mobility or geographic factors (Wan et al. 2025). Furthermore, the rigid assumptions of closed systems exhibit time-varying limitations, failing to represent uncertainties including intervention effects, viral mutations, and temporal fluctuations in real-world epidemic transmission (Du et al. 2024). Given this mismatch, how to propose more generalizable physical priors to guide the design of neural architecture becomes a central challenge.

2) Discrepancy between physical constraints and neural representations. The success of physics-inspired neural networks lies in reconciliation of explicit physical priors with neural representations (Raissi, Perdikaris, and Karniadakis 2019; Chen et al. 2018). For epidemic forecasting, current physics-inspired deep learning methods typically use neural modules to encode the spatio-temporal epidemic patterns and forcibly align the obtained representations with explicit physical quantities (Gao et al. 2021; Kosma et al. 2023). Nevertheless, the latent representation space typically involves nonlinear transformations and combinations, leading to inherent discrepancy when mapped to specific physical variables (Tian et al. 2024). To ensure the model adheres to physical principles while retaining data-driven flexibility, the key architectural design aims to align implicit neural representations with well-established physical meanings (Choi et al. 2023; Verma, Heinonen, and Garg 2024; Hettige et al.

2024), thereby bridging this discrepancy.

In this paper, we present a novel physics-inspired deep learning framework for epidemic dynamics modeling named Epi²-Net, which integrates physical principles of epidemic into neural networks, harmonizing the inconsistency between mechanism-based and data-driven methods. Notably, we reconceptualize epidemic transmission through the lens of physics transport, and establish connections between epidemic modeling and the well-studied diffusion-advection-reaction (DAR) phenomenon (Cosner et al. 2014), which have been rigorously applied in meteorological (Tian et al. 2024; Du et al. 2025) and marine science (Adam and Sibert 2004). Through systematic mapping of physical transport mechanisms to epidemic transmission patterns, we introduce the neural epidemic transport equation to generalize the complexity of real-world epidemic scenarios. Building on the neural epidemic transport equation, we further incorporate a Neural ODE module and neural networks to model spatiotemporal dependencies of epidemics. This design inherently combines physical consistency with adaptability and flexibility of neural representations. Our contributions are summarized as follows:

- We provide a novel view of physical transport for epidemic dynamics modeling and introduce the Neural Epidemic Transport equation to generalize the complexity of real-world epidemic scenarios.
- We propose Epi²-Net, a physics-inspired deep learning framework that synergistically integrates physics priors with neural architectures, unifying interpretable physics guidance with data-driven representational flexibility.
- We conduct experiments on four real-world COVID-19 datasets and show that Epi²-Net outperforms the state-of-the-art competitors in epidemic forecasting task.

2 Related Work

Epidemic Dynamics Modeling

Mechanism-based models. Mechanism-based models integrate physical priors with differential equations to characterize epidemics under idealized conditions, with SIR and its variants being prime examples (Cooper, Mondal, and Antonopoulos 2020). While offering interpretability, they suffer from fundamental limitations of closed-system assumptions (Smith, Moore et al. 2004). The oversimplified physical system demonstrates insufficient generalizability when facing complex, real-world epidemic scenarios. Specifically, the idealized contact assumption neglects natural population mobility (Panagopoulos, Nikolentzos, and Vazirgiannis 2021; Hy et al. 2022) and geographical dependencies (Fan, Varugunda, and Wang 2023), thereby failing to capture urban diffusion dynamics and human activity-driven transmission. Furthermore, factors like viral mutations, vaccine uptake, and policy interventions pose challenges for the real-time calibration of mechanistic methods (Du et al. 2024). Although researchers have attempted to address these issues through mechanistic refinements (Heng and Althaus 2020; Poonia et al. 2022), these adjustments remain inadequate for modeling intricate spatiotemporal patterns and may introduce incorrect inductive biases (Wu et al. 2018).

Data-driven models. Given the intricate interplay of real-world pandemic factors, data-driven models identify latent statistical patterns from observational data to forecast epidemic dynamics. Statistical models such as ARIMA (Kufel 2020) and PROPHET (Mahmud 2020) predict future epidemic trends by analyzing temporal patterns of case number; machine learning models including Linear Regression (Kaur et al. 2022), Random Forest (Galasso, Cao, and Hochberg 2022), and XGBOOST (Fang et al. 2022) enhance forecasting by modeling complex nonlinear relationships in historical observational records; while deep learning techniques (e.g., LSTM, Transformer, and GNN) further capture spatio-temporal transmission patterns from multivariate data sources (Chimmula and Zhang 2020; Liu et al. 2024), such as social determinants (Nguyen et al. 2023), geographical interactions (Fan, Varugunda, and Wang 2023), and regional mobility (Panagopoulos, Nikolentzos, and Vazirgianis 2021). However, purely data-driven approaches risk violating essential epidemiological principles, potentially generating biologically implausible dynamics.

Physics-Inspired Deep Learning

Recent advances prioritize physics-inspired neural networks to combine domain knowledge with powerful deep learning models to solve complex scientific and engineering problems (Karniadakis et al. 2021; Karpatne, Jia, and Kumar 2024). One implementation constrains the loss function with physical priors via penalty terms, ensuring outputs comply with this knowledge but often fragmenting physical constraints from representation learning (Shi, Mo, and Di 2021). More advanced alternatives involve designing hybrid architectures that integrate knowledge into specific model components, thereby bridging the discrepancy between explicit physical equations and implicit neural representations (Verma, Heinonen, and Garg 2024; Hettige et al. 2024; Nascimento et al. 2021). Notably, the continuity equation, renowned for its modeling capacity and extensibility for real-world scenarios, has been widely adopted in this manner across atmospheric sciences (Hettige et al. 2024), marine science (Adam and Sibert 2004) and transportation engineering (Ji et al. 2022). For epidemic dynamics modeling, we pioneer the adoption of physical transport processes, derived from the continuity equation, to guide physics-inspired model design, given the aforementioned two discrepancies for physic-inspired neural methods.

3 Preliminaries

Problem Definition

In this paper, we formulate epidemic dynamics forecasting as a spatio-temporal prediction task. Formally, let $X_{1:T} = \{X_t\}_{t=1}^T \in \mathbb{R}^{N \times D \times T}$ denote historical epidemiological observations, where N is the number of regions, T is the historical time steps, D is the feature dimension ($D = 1$ for daily confirmed cases in our study), and $x_t \in \mathbb{R}^{N \times D}$ is the multivariate regional observations at time t . Let $G = (V, E)$ denote the inter-region graph, where V is the set of regions, E is the set of edges, A denotes the geospatial adjacency matrix of G and $A[i, j]$ denotes the spatial distance between

regions i and j . Moreover, human mobility patterns of regions are defined as $M_{1:T} = \{M_t\}_{t=1}^T \in \mathbb{R}^{N \times N \times T}$, where $M_t[i, j]$ quantifies the mobility from region i to j at time t . The objective is to learn a function $f(\cdot)$ that can accurately predict future epidemic trends over horizon h :

$$\hat{X}_{T+1:T+h} = f(X_{1:T}, M_{1:T}, A). \quad (1)$$

Concepts of Physical Transport

This paper pioneers a physical transport perspective for epidemic modeling. First, we begin by introducing the foundational concepts of physical transport.

Continuity Equation. The continuity equation expresses the conservation of a quantity in a physical system. Specifically, it quantifies the relationship between the temporal variation of system mass and the inflow/outflow of matter:

$$\frac{\partial c}{\partial t} + \nabla \cdot (c\vec{v}) = 0, \quad (2)$$

where c is the fluid density, \vec{v} is the velocity vector, and $\nabla \cdot$ is the divergence operator. Based on this equation, extensive physical transport processes like diffusion, advection, and reaction can be derived.

Diffusion. Diffusion describes the process where particles randomly move from high to low concentration areas in a medium, which can be formulated by continuity equation and Fick's Law (Grady and Polimeni 2010; Paul et al. 2014):

$$\frac{\partial c}{\partial t} \Big|_{diff} - k\nabla^2 c = 0, \quad (3)$$

where k is the diffusion coefficient, and ∇^2 is a Laplacian operator combining divergence and gradient.

Advection. Distinct from the diffusion, advection characterizes the bulk transport of particles driven by an imposed velocity field in fluid systems (Grady and Polimeni 2010):

$$\frac{\partial c}{\partial t} \Big|_{adv} + \vec{v} \cdot \nabla c = 0, \quad (4)$$

where \vec{v} denotes the velocity vector field.

Reaction. Reaction characterizes the localized substance transformations that alter concentrations (Volpert and Petrovskii 2009), governed by:

$$\frac{\partial c}{\partial t} \Big|_{rea} - R(c, t) = 0, \quad (5)$$

where the reaction term $R(\cdot)$ quantifies the source/sink dynamics from physicochemical or other transformations.

Diffusion-Advection-Reaction. Through coupling of diffusion, advection and reaction, we complete the Diffusion-Advection-Reaction (DAR) triad (Cosner et al. 2014):

$$\frac{\partial c}{\partial t} \Big|_{DAR} = \underbrace{k\nabla^2 c}_{diffusion} - \underbrace{\vec{v} \cdot \nabla c}_{advection} + \underbrace{R(c, t)}_{reaction}. \quad (6)$$

Widely applied in various fields, DAR systems in prior works rely on low-dimensional, handcrafted, and non-neural systems, determined by domain experts through trial and error (Adam and Sibert 2004; Khokhlov 1995).

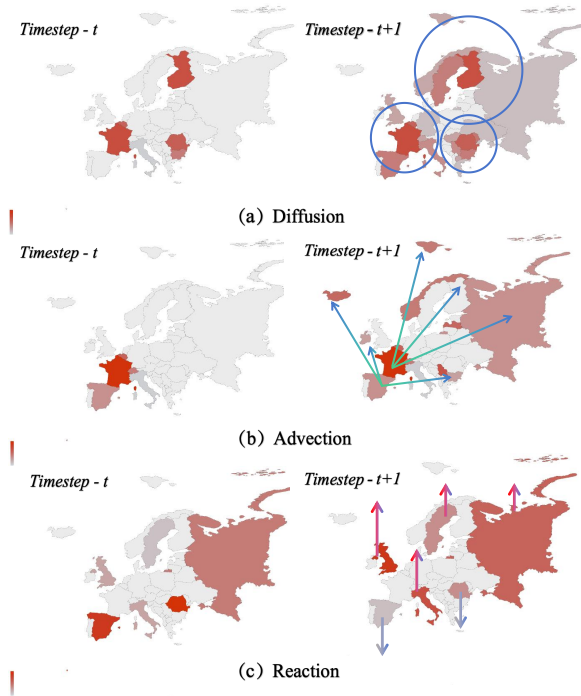


Figure 1: Motivation of introducing physical transport into epidemic dynamics modeling. The heatmaps show infection density for regions at timestep t and $t + 1$. Diffusion illustrates the spread from severely affected regions to neighboring regions; advection captures the spread to specific regions due to human mobility; reaction signifies localized shifts in the regional epidemic, influenced by interventions like lockdown policies, viral mutations, and vaccination.

Neural Epidemic Transport

Inspired by recent studies (Verma, Heinonen, and Garg 2024; Hettige et al. 2024), we view epidemic dynamics as a flux, a spatial movement of quantities over time, for further modeling. To accurately model complex real-world epidemics, we integrate three physical transport processes with the intricacies of epidemic transmission, thereby defining the neural epidemic transport equation. A more intuitive understanding of our motivation is depicted in Figure 1.

Diffusion. The diffusion of epidemics describes the spread from regions with high infection density to neighboring regions with low density, analogous to heat conduction or gas diffusion, with a focus on characterizing the spatial dependence of epidemic transmission. Following (Bronstein et al. 2017), we derive the discrete diffusion equation in terms of the graph Laplacian operator:

$$\left. \frac{\partial X^i}{\partial t} \right|_{dif} = k \cdot \sum_{j \in N(i)} G^{dif}[i, j](X^i - X^j) = k \cdot LX, \quad (7)$$

where X^i denotes the epidemic density of region i , $N(i)$ denotes the neighboring set of i , and $G^{dif}[i, j]$ denotes the transport weight of diffusion from i to j . In our implementation, we compute the spatial distances between re-

gions based on centroid coordinates to establish the diffusion graph $G^{dif}[i, j] = \frac{1}{d_{ij}}$, where d_{ij} is the haversine distance between regions i and j . L denotes the normalized graph Laplacian matrix, derived from the static G^{dif} (equivalent to the geospatial adjacency matrix A).

Advection. The advection of epidemics refers to the rapid, cross-regional transmission of pathogens driven by large-scale, directional population movements (e.g., transportation, migration), analogous to the pollutant transport driven by river currents or atmospheric flow, with particular emphasis on characterizing the spatio-temporal dynamics of pandemic transmission. Following (Chapman 2015), the discrete analogue of advection can be formulated as:

$$\left. \frac{\partial X^i}{\partial t} \right|_{adv} = \sum_{\forall j|j \rightarrow i} G^{adv}[j, i]X^j - \sum_{\forall i|i \leftarrow k} G^{adv}[i, k]X^i, \quad (8)$$

where $G^{adv}[i, j]$ denotes the transport weight of advection from region i to j . As population movement as a critical factor in epidemic spread, we model the human mobility as the flow field in advection, following (Hettige et al. 2024). This allows us to construct the advection graph using inter-regional human flow data:

$$\left. \frac{\partial X}{\partial t} \right|_{adv} = M_t X, \quad (9)$$

where M_t quantifies the cross-regional mobility at time t , and M includes dynamic and directed graph snapshots.

Reaction. The reaction of epidemics indicates the complex intra-regional dynamics, such as localized lockdowns, vaccination campaigns, herd immunity, and viral variants, which depend on both biological factors and social determinants in real-world scenarios. Distinct from diffusion and advection, the reaction primarily models endogenous patterns within a region, which can be analogized to autocatalytic and equilibrium inhibition phenomena of chemical reactions (Bissette and Fletcher 2013; Lewis 1925):

$$\left. \frac{\partial X}{\partial t} \right|_{rea} = R(X), \quad (10)$$

where $R(\cdot)$ denotes the reaction term. Given the flexibility of localized dynamics, modeling it using learnable parameters through neural network is a viable approach (Du et al. 2025).

Neural epidemic transport equation. Based on the previous discussion, we introduce the neural epidemic transport equation, which unifies real-world epidemic complexity including geographic dependencies, human mobility, and localized reaction dynamics:

$$\frac{\partial X}{\partial t} = \mu \odot \left. \frac{\partial X}{\partial t} \right|_{dif} + (1 - \mu) \odot \left. \frac{\partial X}{\partial t} \right|_{adv} + \gamma \odot \left. \frac{\partial X}{\partial t} \right|_{rea}, \quad (11)$$

where μ and γ are learnable coefficients obtained by neural networks. Given the intricate interplay between diffusion and advection in particle transport (Hettige et al. 2024), we incorporate a learnable parameter μ for adaptive fusion to highlight inter-regional patterns. Concurrently, under an open-system assumption (Tian et al. 2024), the reaction parameter γ prioritizes the intra-regional epidemic modeling.

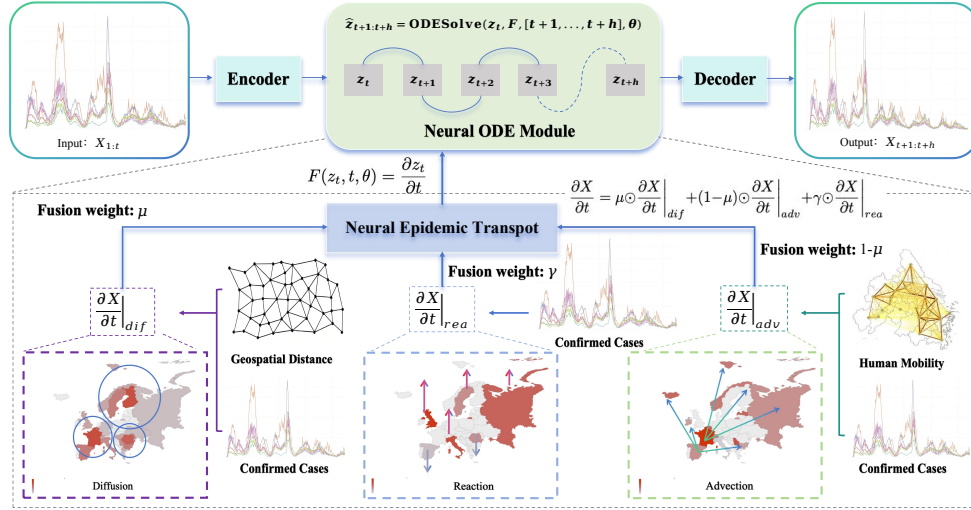


Figure 2: The overall framework of Epi²-Net consists of three components: 1) an encoder to model temporal dependency from the historical observations, 2) a Neural ODE module to model the evolution of epidemic dynamics, 3) a decoder to generate predictions of epidemic trends based on the neural representations and physical priors.

Physics-Informed Neural Framework

Based on the neural epidemic transport, we further introduce the physics-inspired neural framework, Epi²-Net, which includes three main components: an encoder, a Neural ODE module, and a decoder. The overall architecture of Epi²-Net is depicted in Figure 2.

Encoder. To fully leverage the data-driven flexibility, we employ a neural encoder to extract temporal dependencies from the historical epidemic observations, and obtain the initial state for neural ODE module (Chen et al. 2018):

$$z_t = \text{Encoder}(X_{t-w:t}), \quad (12)$$

where w denotes the observation window length. Following prior studies (Ji et al. 2022; Hettige et al. 2024), we implement the encoder by a RNN-based module combined with a reparameterization trick (Kingma, Welling et al. 2013).

Neural ODE Module. To integrate physics constraints into neural framework, we draw inspiration from Neural ODEs (Chen et al. 2018) and introduce the neural epidemic transport to guide the module design. Specifically, our Neural ODE vector field $F(\cdot)$ is formulated using the discretized graph operators and reaction term, as follows:

$$F(z_t, t, \theta) = \frac{\partial z_t}{\partial t} = \mu \odot (-k \cdot LX) - (1 - \mu) \odot (MX) + \gamma \odot X, \quad (13)$$

where \odot is the hadamard product operation, θ denotes learnable parameters to approximate the neural epidemic transport. The diffusion coefficient k and reaction coefficient γ are updated by neural networks. Moreover, the fusion weight μ is obtained by a fully-connected layer, leveraging neural representations of diffusion and advection branches. After reconciling physical priors with neural representations, we apply the Neural ODE solver to compute the future states:

$$\hat{z}_{t+1:t+h} = \text{ODESolve}(z_t, F, [t+1, \dots, t+h], \theta). \quad (14)$$

Decoder. Finally, a decoder generates epidemic predictions from the latent representation. Consistent with (Hettige et al. 2024; Ji et al. 2022), we utilize the non-neural decoding operation (reshaping and aggregation) to produce the output format at each time step:

$$\hat{X}_{t+1:t+h} = \text{Decoder}(\hat{z}_{t+1:t+h}). \quad (15)$$

Subsequently, we optimize Epi²-Net via back-propagation to minimize the Root Mean Square Error (RMSE) function:

$$\mathcal{L} = \sqrt{\frac{1}{h} \sum_{k=t+1}^{t+h} \|X_k - \hat{X}_k\|_2^2}. \quad (16)$$

4 Experiments

Experimental Settings

Datasets. We evaluate our proposed Epi²-Net on four real-world COVID-19 datasets: England, France, Italy, and Spain (Panagopoulos, Nikolentzos, and Vazirgiannis 2021). The dataset comprises three main components: daily cases, human mobility, and geographical distances. We obtained daily cases and human mobility data from open-source GitHub repository¹, and manually constructed geographical distance information. According to (Hy et al. 2022; Nguyen et al. 2023; Gong et al. 2025), we employ the daily reported case as the epidemic feature. The target is to forecast the new cases in specific regions for given countries. Basic statistics of dataset and further details are provided in Appendix A.

Settings and implementations. To comprehensively evaluate Epi²-Net, we conduct epidemic predictions across three horizons: 3 days, 5 days, and 7 days. We split each dataset chronologically in the ratio of 60%:20%:20% to generate

¹https://github.com/geopanag/pandemic_tgnn

training, validation, and test sets respectively. To evaluate performance, we use Mean Absolute Error (MAE) and Root Mean Square Error (RMSE) as metrics (see in Appendix B). More implementation details are provided in Appendix C.

Baselines. We evaluate Epi²-Net against 14 representative baselines from four categories: 1) **Statistical methods:** HA (Historical Average), PROPHET (Mahmud 2020), and ARIMA (Kufel 2020). 2) **Machine learning methods:** LIN_REG (Kaur et al. 2022), RAND_FOREST (Galasso, Cao, and Hochberg 2022) XGBOOST (Fang et al. 2022). 3) **Deep learning methods:** ITRANSFORMER (Liu et al. 2023), TIMEMIXER (Wang et al. 2024), STGNN (Kapoor et al. 2020), ATMGNN (Nguyen et al. 2023) 4) **Physics-inspired neural methods:** ODE-LSTM (Lechner and Hasani 2020), GN-ODE (Kosma et al. 2023), EINNs (Rodríguez et al. 2023), EARTH (Wan et al. 2025). More baseline details are provided in Appendix D.

Performance Comparison

From Table 1, we can observe that: 1) Epi²-Net consistently outperforms all baselines across every dataset, achieving a remarkable 21.03% improvement in MAE over the best-performing baseline on France-7days. 2) deep learning methods, particularly TIMEMIXER and ATMGNN, outperform statistical and machine learning methods, demonstrate powerful modeling capabilities in capturing complex real-world epidemics. 3) physic-inspired neural methods such as EPINNs and EARTH exhibit competitive performance, indicating benefits of integrating physic priors into neural architectures. 4) the suboptimal performance of physics-inspired neural methods such as ODE-LSTM and GN-ODE stems from oversimplified physical priors, which cannot adapt to multifaceted factors in real-world settings. Additional experiments on metric RMSE are provided in Appendix E.

Case Study

The case study in Figure 3 visualizes the epidemic dynamics of COVID-19 in France. We primarily focuses on three key areas: north, southwest, and southeast regions. In the early stages of the outbreak (May 10th), EpiNet’s predictions already provided early warnings for three major areas. By the full escalation of the epidemic (May 12th), EpiNet accurately predicted severely affected areas, supporting precise interventions. We also visualized the learned γ values in Figure 4(a) for each region in France, and performed a fine-grained analysis of Paris and Bouches-du-Rhône (BdR), two regions with the largest γ . Figures 4(b) and 4(c) show the new cases for Paris and BdR, indicating that the infection levels in these two regions far exceed the average for all of France, and the interpretability of reaction coefficients. For more case study and analysis, please refer to Appendix F.

Ablation Study

Physical transport processes. To quantify the contribution of physical priors, we compare Epi²-Net against six variants: 1) Dif-Only: only the diffusion process. 2) Adv-Only: only the advection process. 3) Rea-Only: only the reaction process. 4) Dif-Adv: the diffusion and advection

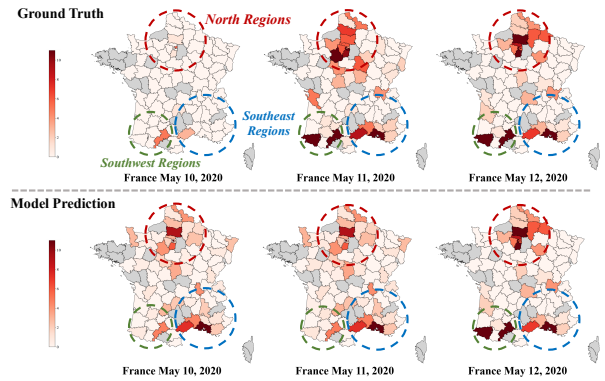


Figure 3: A case study examines COVID-19 progression in partial regions of France. Gray shading denotes areas lacking surveillance records.

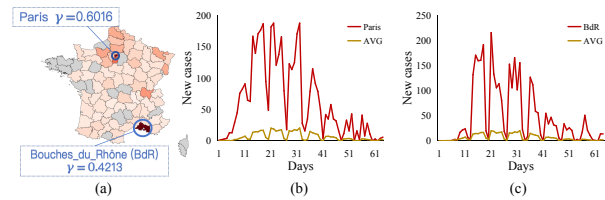


Figure 4: Visualization of γ values and the infection status of two critical regions: Paris and Bouches-du-Rhône (BdR).

processes. 5) Dif-Rea: the diffusion and reaction processes. 6) Adv-Rea: the advection and reaction processes. Figure 5 shows the comparison results on France and Italy, we observe that Epi²-Net achieve the best performance, indicating the significance of integrating comprehensive physic priors (diffusion, advection, and reaction) into epidemic modeling. Evidently, using single transport process (Dif-Only, Adv-Only, and Rea-Only) as the prior significantly degrades the performance. While integrating two transport processes (Dif-Adv, Dif-Rea, and Adv-Rea) significantly improves the forecasting accuracy compared to single-process models, the performance remains inferior to Epi²-Net, reaffirming the importance of the complete neural epidemic transport.

Temporal encoder. To study the efficacy of the encoder, we compare our model with three variants: 1) LSTM: adopt the LSTM (Hochreiter and Schmidhuber 1997) as the encoder. 2) TCN: adopt the Temporal Convolutional Network (Bai, Kolter, and Koltun 2018) as encoder. 3) Transformer: adopt the Transformer (Vaswani et al. 2017) block as encoder. 4) GRU: adopt the Gated Recurrent Unit (Chung et al. 2014) as encoder. Based on Table 2, GRU temporal encoders are advantageous, as advanced architecture Transformer lose their long-range dependency modeling benefits in this scenario. For additional experiments of encoder and decoder, please refer to Appendix G.

Model Stability Analysis

ODE solver stability. To evaluated the computational robustness and runtime differences of Epi²-Net, we implement

Table 1: The overall performance comparison of epidemic dynamics forecasting on metric MAE. The bold and underlined fonts show the best and the second best result. The improvement(%) is calculated based on these two results.

Model	England			France			Italy			Spain		
	3 days	5 days	7 days	3 days	5 days	7 days	3 days	5 days	7 days	3 days	5 days	7 days
HA	7.24	7.63	7.97	6.03	6.08	6.21	30.89	30.69	29.59	74.03	74.35	74.27
PROPHET	10.19	10.52	14.39	8.07	8.17	8.41	46.79	50.05	51.29	85.59	86.99	86.57
ARIMA	8.13	8.08	8.72	6.02	6.24	6.34	45.81	46.29	47.52	84.32	85.53	85.01
LIN_REG	8.40	9.10	10.11	6.74	6.68	6.20	31.94	32.50	33.29	72.39	73.45	78.05
RAND_FOREST	7.52	7.18	7.00	4.17	4.05	4.53	29.37	29.42	29.17	53.32	55.81	53.42
XGBOOST	7.40	6.76	7.09	4.56	4.97	4.86	27.75	28.18	28.60	50.07	50.74	52.55
ITRANSFORMER	6.12	6.26	6.45	2.93	3.04	3.13	21.09	21.52	21.58	29.91	30.53	30.95
TIMEMIXER	5.95	6.16	6.31	2.86	3.07	3.29	21.08	21.46	21.80	28.85	28.13	28.44
STGNN	6.70	6.77	6.56	3.66	3.20	3.35	25.89	26.72	26.85	27.55	27.33	27.06
ATMGNN	6.08	6.21	6.08	3.44	3.34	3.09	24.63	24.68	24.02	26.05	26.52	26.74
ODE-LSTM	8.15	8.39	8.66	5.04	5.21	5.84	30.82	30.77	31.05	41.94	42.00	42.08
GN-ODE	8.25	8.48	9.54	5.92	5.87	5.91	27.57	27.01	27.90	42.63	41.99	47.70
EPINNs	7.23	8.63	8.72	3.02	3.99	3.92	21.02	2.32	21.57	28.95	28.24	28.99
EARTH	5.96	6.05	6.22	3.96	3.78	3.49	20.05	20.37	20.74	26.61	26.75	26.93
Epi ² -Net	5.35	5.50	5.70	2.55	2.62	2.44	18.14	18.21	18.53	25.59	25.19	24.18
Improvement(%)	10.08	9.09	6.25	10.84	14.65	21.03	9.52	10.60	10.65	1.76	5.01	9.57

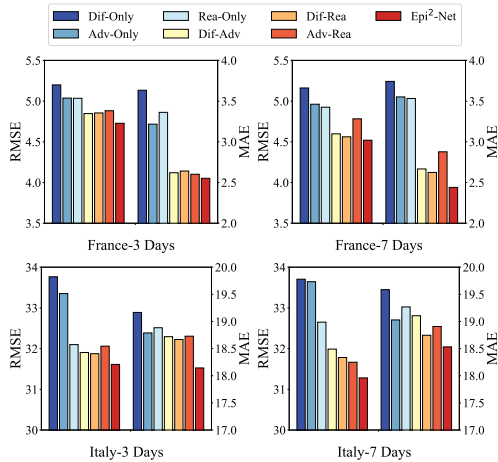


Figure 5: Ablation study on physical transport processes.

Table 2: Performance comparison of temporal encoder.

Encoder	England-3days		Spain-5days		Italy-7days	
	RMSE	MAE	RMSE	MAE	RMSE	MAE
LSTM	7.68	5.46	47.40	36.81	34.79	21.54
TCN	8.58	6.56	54.70	38.89	33.30	21.23
Transformer	9.32	7.63	41.77	34.02	33.62	25.18
GRU	7.57	5.35	40.77	25.59	31.28	18.53

Table 3: Performance comparison of different ODE solvers.

ODE Solver	England		Italy		Inference Phase	
	RMSE	MAE	RMSE	MAE	Time (s)	Speedup
Euler	8.09	5.69	31.28	18.54	0.52	1.00×
Bosh3	8.08	5.69	31.28	18.54	0.70	0.74×
Rk4	8.08	5.67	31.28	18.53	0.71	0.73×
Dopri5	8.08	5.67	31.28	18.53	0.97	0.54×

the model via four distinct numerical solvers (Euler, Bosh3, Rk4, and Dopri5). Table 3 shows the performance comparison of different ODE solvers, note that the inference time here refers to the runtime on the test set. We observe that Epi²-Net exhibits consistent performance across various numerical solvers. Both Rk4 and Dopri5, as high-order Runge-Kutta solvers, demonstrate superior performance compared to lower-order methods. We recommend them since their accuracy improvements justify the computational investment for precision-critical forecasting.

Numerical stability. Given Epi²-Net’s integration of neural ODE module, a temporal encoder, learnable coefficients and a fully-connected layer, its numerical stability must be verified. Detailed numerical stability analysis and additional stability experiments are presented in Appendix H.

5 Conclusions

In this paper, we present Epi²-Net, a physic-inspired deep learning framework to advance epidemic dynamics modeling. By integrating physical priors into neural architecture, we introduce the neural epidemic transport to build upon Epi²-Net, and reconcile explicit physical prior with neural representations. Extensive experiment results have demonstrated its superior performance for epidemic forecasting.

6 Limitations and Future Works

Although Epi²-Net integrates case numbers, human mobility, and geographical data, epidemic modeling is a complex problem. Government policies, viral mutation, emergent outbreak, etc., are all key factors for real-world epidemics. The current framework struggles to achieve broad integration. Since it cannot fully unlock the potential of data-driven paradigm, combining advanced architectures (Transformer, LLM) with broader multifaceted data is a promising direction. Further discussions are provided in Appendix I.

References

- Adam, M. S.; and Sibert, J. R. 2004. Use of neural networks with advection-diffusion-reaction models to estimate large-scale movements of Skipjack tuna from tagging data. Technical report, Marine Research Centre, Ministry of Fisheries, Agriculture and Marine Resources.
- Al-Aly, Z.; Davis, H.; McCorkell, L.; Soares, L.; Wulf-Hanson, S.; Iwasaki, A.; and Topol, E. J. 2024. Long COVID science, research and policy. *Nature medicine*, 30(8): 2148–2164.
- Azevedo, J. P. W. D.; Rogers, F. H.; Ahlgren, S. E.; Cloutier, M.-H.; Chakroun, B.; Chang, G.-C.; Mizunoya, S.; Reuge, N. J.; Brossard, M.; and Bergmann, J. L. 2021. The State of the Global Education Crisis: A Path to Recovery (Vol. 2): Executive Summary (Portuguese).
- Bai, S.; Kolter, J. Z.; and Koltun, V. 2018. An empirical evaluation of generic convolutional and recurrent networks for sequence modeling. *arXiv preprint arXiv:1803.01271*.
- Bauer, P.; Thorpe, A.; and Brunet, G. 2015. The quiet revolution of numerical weather prediction. *Nature*, 525(7567): 47–55.
- Bissette, A. J.; and Fletcher, S. P. 2013. Mechanisms of autocatalysis. *Angewandte Chemie International Edition*, 52(49): 12800–12826.
- Bronstein, M. M.; Bruna, J.; LeCun, Y.; Szlam, A.; and Vandergheynst, P. 2017. Geometric deep learning: going beyond euclidean data. *IEEE Signal Processing Magazine*, 34(4): 18–42.
- Chapman, A. 2015. Advection on graphs. In *Semi-autonomous networks: Effective control of networked systems through protocols, design, and modeling*, 3–16. Springer.
- Chen, R. T.; Rubanova, Y.; Bettencourt, J.; and Duvenaud, D. K. 2018. Neural ordinary differential equations. *Advances in neural information processing systems*, 31.
- Chimmula, V. K. R.; and Zhang, L. 2020. Time series forecasting of COVID-19 transmission in Canada using LSTM networks. *Chaos, solitons & fractals*, 135: 109864.
- Choi, H.; Choi, J.; Hwang, J.; Lee, K.; Lee, D.; and Park, N. 2023. Climate modeling with neural advection–diffusion equation. *Knowledge and Information Systems*, 65(6): 2403–2427.
- Chung, J.; Gulcehre, C.; Cho, K.; and Bengio, Y. 2014. Empirical evaluation of gated recurrent neural networks on sequence modeling. *arXiv preprint arXiv:1412.3555*.
- Cooper, I.; Mondal, A.; and Antonopoulos, C. G. 2020. A SIR model assumption for the spread of COVID-19 in different communities. *Chaos, Solitons & Fractals*, 139: 110057.
- Cosner, C.; et al. 2014. Reaction-diffusion-advection models for the effects and evolution of dispersal. *Discrete Contin. Dyn. Syst.*, 34(5): 1701–1745.
- Du, H.; Zhao, J.; Zhao, Y.; Xu, S.; Lin, X.; Chen, Y.; Gardner, L. M.; and Yang, H. F. 2024. Advancing real-time pandemic forecasting using large language models: A covid-19 case study. *arXiv preprint arXiv:2404.06962*.
- Du, S.; Wei, H.; Lee, D. Y.; Hu, Z.; and Pan, S. 2025. Graph-Based Physics-Guided Urban PM_{2.5} Air Quality Imputation with Constrained Monitoring Data. *ACM Transactions on Sensor Networks*.
- Fan, C.-H.; Varugunda, S. S.; and Wang, L. 2023. Exploring Graph Structure in Graph Neural Networks for Epidemic Forecasting. In *Temporal Graph Learning Workshop@ NeurIPS 2023*.
- Fang, Z.-g.; Yang, S.-q.; Lv, C.-x.; An, S.-y.; and Wu, W. 2022. Application of a data-driven XGBoost model for the prediction of COVID-19 in the USA: a time-series study. *BMJ open*, 12(7): e056685.
- Galasso, J.; Cao, D. M.; and Hochberg, R. 2022. A random forest model for forecasting regional COVID-19 cases utilizing reproduction number estimates and demographic data. *Chaos, Solitons & Fractals*, 156: 111779.
- Gao, J.; Sharma, R.; Qian, C.; Glass, L. M.; Spaeder, J.; Romberg, J.; Sun, J.; and Xiao, C. 2021. STAN: spatio-temporal attention network for pandemic prediction using real-world evidence. *Journal of the American Medical Informatics Association*, 28(4): 733–743.
- Gong, C.; Sun, R.; Zheng, Y.; Zhang, J.; Gu, T.; Pan, L.; and Lv, L. 2025. EpiLLM: Unlocking the Potential of Large Language Models in Epidemic Forecasting. *arXiv preprint arXiv:2505.12738*.
- Grady, L. J.; and Polimeni, J. R. 2010. Discrete calculus: History and future. In *Discrete Calculus: Applied Analysis on Graphs for Computational Science*, 1–9. Springer.
- Heng, K.; and Althaus, C. L. 2020. The approximately universal shapes of epidemic curves in the Susceptible-Exposed-Infectious-Recovered (SEIR) model. *Scientific Reports*, 10(1): 19365.
- Hettige, K. H.; Ji, J.; Xiang, S.; Long, C.; Cong, G.; and Wang, J. 2024. Airphynet: Harnessing physics-guided neural networks for air quality prediction. *arXiv preprint arXiv:2402.03784*.
- Hochreiter, S.; and Schmidhuber, J. 1997. Long short-term memory. *Neural computation*, 9(8): 1735–1780.
- Hy, T. S.; Nguyen, V. B.; Tran-Thanh, L.; and Kondor, R. 2022. Temporal multiresolution graph neural networks for epidemic prediction. In *Workshop on Healthcare AI and COVID-19*, 21–32. PMLR.
- Ji, J.; Wang, J.; Jiang, Z.; Jiang, J.; and Zhang, H. 2022. STDEN: Towards physics-guided neural networks for traffic flow prediction. In *Proceedings of the AAAI conference on artificial intelligence*, volume 36, 4048–4056.
- Jordà, Ò.; Singh, S. R.; and Taylor, A. M. 2022. Longer-run economic consequences of pandemics. *Review of Economics and Statistics*, 104(1): 166–175.
- Kapoor, A.; Ben, X.; Liu, L.; Perozzi, B.; Barnes, M.; Blais, M.; and O’Banion, S. 2020. Examining covid-19 forecasting using spatio-temporal graph neural networks. *arXiv preprint arXiv:2007.03113*.
- Karniadakis, G. E.; Kevrekidis, I. G.; Lu, L.; Perdikaris, P.; Wang, S.; and Yang, L. 2021. Physics-informed machine learning. *Nature Reviews Physics*, 3(6): 422–440.

- Karpatne, A.; Jia, X.; and Kumar, V. 2024. Knowledge-guided machine learning: Current trends and future prospects. *arXiv preprint arXiv:2403.15989*.
- Kaur, G.; Kaur, P.; Kaur, N.; and Kaur, P. 2022. Forecasting Prediction of Covid-19 Outbreak Using Linear Regression. In *Data Intelligence and Cognitive Informatics: Proceedings of ICDICI 2022*, 195–221. Springer.
- Khokhlov, A. M. 1995. Propagation of turbulent flames in supernovae. *Astrophysical Journal* v. 449, p. 695, 449: 695.
- Kingma, D. P.; Welling, M.; et al. 2013. Auto-encoding variational bayes.
- Kosma, C.; Nikolentzos, G.; Panagopoulos, G.; Steyaert, J.-M.; and Vazirgiannis, M. 2023. Neural ordinary differential equations for modeling epidemic spreading. *Transactions on Machine Learning Research*.
- Kufel, T. 2020. ARIMA-based forecasting of the dynamics of confirmed Covid-19 cases for selected European countries. *Equilibrium. Quarterly Journal of Economics and Economic Policy*, 15(2): 181–204.
- Lechner, M.; and Hasani, R. 2020. Learning long-term dependencies in irregularly-sampled time series. *arXiv preprint arXiv:2006.04418*.
- Lewis, G. N. 1925. A new principle of equilibrium. *Proceedings of the National Academy of Sciences*, 11(3): 179–183.
- Liu, Y.; Hu, T.; Zhang, H.; Wu, H.; Wang, S.; Ma, L.; and Long, M. 2023. itransformer: Inverted transformers are effective for time series forecasting. *arXiv preprint arXiv:2310.06625*.
- Liu, Z.; Wan, G.; Prakash, B. A.; Lau, M. S.; and Jin, W. 2024. A review of graph neural networks in epidemic modeling. In *Proceedings of the 30th ACM SIGKDD Conference on Knowledge Discovery and Data Mining*, 6577–6587.
- Mahmud, S. 2020. Bangladesh COVID-19 daily cases time series analysis using Facebook prophet model. Available at SSRN 3660368.
- Nascimento, R. G.; Corbetta, M.; Kulkarni, C. S.; and Viana, F. A. 2021. Hybrid physics-informed neural networks for lithium-ion battery modeling and prognosis. *Journal of Power Sources*, 513: 230526.
- Nguyen, V. B.; Hy, T. S.; Tran-Thanh, L.; and Nghiem, N. 2023. Predicting COVID-19 pandemic by spatio-temporal graph neural networks: A New Zealand’s study. *arXiv preprint arXiv:2305.07731*.
- Panagopoulos, G.; Nikolentzos, G.; and Vazirgiannis, M. 2021. Transfer graph neural networks for pandemic forecasting. In *Proceedings of the AAAI Conference on Artificial Intelligence*, volume 35, 4838–4845.
- Paul, A.; Laurila, T.; Vuorinen, V.; and Divinski, S. V. 2014. *Thermodynamics, diffusion and the Kirkendall effect in solids*. Springer.
- Poonia, R. C.; Saudagar, A. K. J.; Altameem, A.; Alkhatami, M.; Khan, M. B.; and Hasanat, M. H. A. 2022. An enhanced SEIR model for prediction of COVID-19 with vaccination effect. *Life*, 12(5): 647.
- Punn, N. S.; Sonbhadra, S. K.; and Agarwal, S. 2020. COVID-19 epidemic analysis using machine learning and deep learning algorithms. *MedRxiv*, 2020–04.
- Raissi, M.; Perdikaris, P.; and Karniadakis, G. E. 2019. Physics-informed neural networks: A deep learning framework for solving forward and inverse problems involving nonlinear partial differential equations. *Journal of Computational physics*, 378: 686–707.
- Rodríguez, A.; Cui, J.; Ramakrishnan, N.; Adhikari, B.; and Prakash, B. A. 2023. Einns: epidemiologically-informed neural networks. In *Proceedings of the AAAI conference on artificial intelligence*, volume 37, 14453–14460.
- Shi, R.; Mo, Z.; and Di, X. 2021. Physics-informed deep learning for traffic state estimation: A hybrid paradigm informed by second-order traffic models. In *Proceedings of the AAAI Conference on Artificial Intelligence*, volume 35, 540–547.
- Smith, D.; Moore, L.; et al. 2004. The SIR model for spread of disease—the differential equation model. *Convergence*, 3.
- Tian, J.; Liang, Y.; Xu, R.; Chen, P.; Guo, C.; Zhou, A.; Pan, L.; Rao, Z.; and Yang, B. 2024. Air quality prediction with physics-guided dual neural odes in open systems. *arXiv preprint arXiv:2410.19892*.
- Vaswani, A.; Shazeer, N.; Parmar, N.; Uszkoreit, J.; Jones, L.; Gomez, A. N.; Kaiser, Ł.; and Polosukhin, I. 2017. Attention is all you need. *Advances in neural information processing systems*, 30.
- Verma, Y.; Heinonen, M.; and Garg, V. 2024. Climode: Climate and weather forecasting with physics-informed neural odes. *arXiv preprint arXiv:2404.10024*.
- Volpert, V.; and Petrovskii, S. 2009. Reaction–diffusion waves in biology. *Physics of life reviews*, 6(4): 267–310.
- Wan, G.; Liu, Z.; Shan, X.; Lau, M. S.; Prakash, B. A.; and Jin, W. 2025. EARTH: Epidemiology-Aware Neural ODE with Continuous Disease Transmission Graph. In *Forty-second International Conference on Machine Learning*.
- Wang, P.; Zheng, X.; Li, J.; and Zhu, B. 2020. Prediction of epidemic trends in COVID-19 with logistic model and machine learning technics. *Chaos, Solitons & Fractals*, 139: 110058.
- Wang, S.; Wu, H.; Shi, X.; Hu, T.; Luo, H.; Ma, L.; Zhang, J. Y.; and Zhou, J. 2024. Timemixer: Decomposable multiscale mixing for time series forecasting. *arXiv preprint arXiv:2405.14616*.
- Wu, Y.; Yang, Y.; Nishiura, H.; and Saitoh, M. 2018. Deep learning for epidemiological predictions. In *The 41st international ACM SIGIR conference on research & development in information retrieval*, 1085–1088.
- Xie, Y.; Xu, E.; Bowe, B.; and Al-Aly, Z. 2022. Long-term cardiovascular outcomes of COVID-19. *Nature medicine*, 28(3): 583–590.
- Zhou, X.; Zhou, J.; Wang, C.; Xie, Q.; Ding, K.; Mao, C.; Liu, Y.; Cao, Z.; Chu, H.; Chen, X.; et al. 2025. PH-LLM: Public Health Large Language Models for Inveillance. *medRxiv*.

A Further Details of Datasets

Datasets description. The COVID-19, first detected in Wuhan, China in December 2019, is caused by the novel severe acute respiratory syndrome coronavirus 2 (SARS-CoV-2), which shares genetic similarities with bat coronaviruses, pangolin coronaviruses, and SARS-CoV. In this paper, we focus on the COVID-19 epidemic dynamics in selected European countries: England, France, Italy, and Spain. The dataset comprises three primary components: daily cases, human mobility, and geographical distances. Basic statistics of datasets are summarized in Table 4.

Daily cases. Daily confirmed case numbers across part administrative regions of the four study countries are extracted from open-source GitHub repository².

Human mobility. Raw data of human mobility are obtained from anonymized mobile device signals collected through the Facebook App (with user consent and location history enabled), available via a GitHub repository³. The raw dataset contains tri-daily population movement volumes (recorded at midnight, morning, and afternoon) between regions. Following prior studies (Panagopoulos, Nikolentzos, and Vazirgiannis 2021), we aggregated the three measurements into a single inter-regional mobility metric.

Geographical distances. The inter-regional geographical distances are calculated via centroid coordinates (latitude/longitude) obtained from OpenStreetMap⁴, with spatial distance measurements computed via the Haversine formula.

Table 4: The statistics information of datasets in epidemic dynamics forecasting for COVID-19.

Dataset	Observation Period	#Regions	Avg.Cases
England	2020-03-13 – 2020-05-12	129	16.7
France	2020-03-10 – 2020-05-12	81	7.5
Italy	2020-02-24 – 2020-05-12	105	25.65
Spain	2020-03-12 – 2020-05-12	34	61

B Evaluation Metrics

Let $\mathbf{x} = (x_1, x_2, \dots, x_n)$ denotes the ground truth, and $\hat{\mathbf{x}} = (\hat{x}_1, \hat{x}_2, \dots, \hat{x}_n)$ represents the predicted result. The evaluation metrics for one region we used in this paper are defined as follows:

Mean Absolute Error (MAE).

$$MAE(\mathbf{x}, \hat{\mathbf{x}}) = \frac{1}{n} \sum_{i=1}^n |x_i - \hat{x}_i| \quad (17)$$

Root Mean Square Error (RMSE).

$$RMSE(\mathbf{x}, \hat{\mathbf{x}}) = \sqrt{\frac{1}{n} \sum_{i=1}^n (x_i - \hat{x}_i)^2} \quad (18)$$

²<https://dataforgood.fb.com/tools/disease-prevention-maps/>

³https://github.com/geopanag/pandemic_tgnn

⁴<https://www.openstreetmap.org>

C Implementation Details

Model implementation. Epi²-Net is implemented in PyTorch 2.5.1 using NVIDIA GeForce RTX 4090 GPU. In the default settings, we use GRU to implement the RNN-based encoder and adopt a non-neural decoder. We follow (Hettige et al. 2024) and implement the graph Laplacian operators of the Neural ODE module in the form of GCN layers. For the ODESolver, we use Dopri5, an explicit Runge-Kutta method. Moreover, models involving neural network modules in the baseline are subjected to five experimental runs, and their average results are reported for evaluation.

Hyperparameter settings. We tune the key hyperparameters in our implementation to achieve optimal model performance. We set the batch size to 32, and the initial learning rate to 5e-2. We set the GRU encoder hidden dimension to 16, and the observation window length w of encoder to 7. We used the Adam optimizer with a MultiStepLR learning rate scheduling strategy. The model was trained for a maximum of 100 epochs, with an early stopping patience of 10. During the encoding process, we employ the reparameterization trick (Ji et al. 2022; Hettige et al. 2024) and generate multiple samples from the latent trajectory to model uncertainty and provide a more robust prediction. The relative and absolute tolerances (rtol and atol) of ODESolver for Dopri5 are set to 1e-5. The following list details the search space for each hyperparameter and the final selected optimal values:

- Learning rate (lr): {1e-1, **5e-2**, 1e-2, 5e-3, 1e-3}
- Lr scheduler gamma: {0.1, 0.3, **0.5**, 0.7}
- Lr scheduler milestones: {[25, 50, 75], [**25, 35, 45, 55**], [20, 40, 60, 80]}
- Batch size: {8, **16**, 32, 64}
- Hidden dimension of encoder: {8, **16**, 32, 64}

Datasets splits. Epidemic forecasting tasks for COVID-19, characterized by rapid outbreak and swift transmission, typically involve spatiotemporal sequences spanning approximately 60 days. Incompatible with conventional cross-validation settings, we adopt a temporally ordered dataset partitioning strategy, better aligning with real-world epidemic scenarios. Specifically, for our spatiotemporal sequences, we employ a sliding window strategy and partition the data chronologically into training, validation, and testing sets according to a 6:2:2 ratio. This ensures that the validation and test sets are of sufficient size for reliable model selection and performance evaluation, and the entire process strictly adheres to the temporal causality inherent in real-world forecasting tasks.

D Further Details of Baselines

To evaluate Epi²-Net, we conducted a comparative analysis with 14 methods in epidemic forecasting. The models we benchmark against are as follows:

- HA (Historical Average): The epidemic prediction result is derived by averaging the observed cases.
- PROPHET (Mahmud 2020): A time-series model where the input is the history of entire reported cases for each region, which is widely used in epidemic forecasting.

- ARIMA (Kufel 2020): An autoregressive moving average model for time-series forecasting, which the input is similar to PROPHET.
- LIN_REG (Kaur et al. 2022): Given the history of reported cases for each region as input, ordinary least squares linear regression is used to fit the line of cases on the training sets to forecast the future epidemic trend.
- RAND_FOREST (Galasso, Cao, and Hochberg 2022): A random forest regression model that produces epidemic forecasting using decision trees, with multiple trees built based on the training sets to best average the final results.
- XGBOOST (Fang et al. 2022): An enhanced version of random forest regression model for epidemic forecasting via gradient boosting.
- ITRANSFORMER (Liu et al. 2023): iTransformer reverses the conventional Transformer’s method of processing time series data, redirecting attention from the temporal axis to the feature axis. This framework is then utilized to model the time evolution of case counts for epidemic forecasting.
- TIMEMIXER (Wang et al. 2024): TimeMixer is built upon MLPs, avoiding complex self-attention mechanisms or recurrent structures. It models time series data through multiscale series decomposition and a disentangled mixing strategy. Based on TimeMixer, we model the temporal pattern of case counts for epidemic forecasting.
- STGNN (Kapoor et al. 2020): This method models human mobility, inter-region connectivity, and epidemic evolution patterns within the epidemic using Spatio-Temporal Graph Neural Networks, to further predict the epidemic.
- ATMGNN (Nguyen et al. 2023): A hybrid deep learning model for epidemic forecasting, where multiple resolution GNN are combined with Transformers for modeling the epidemics.
- ODE-LSTM (Lechner and Hasani 2020): ODE-LSTM combines RNN structures with Neural ODEs, allowing for the encoding of a continuous-time dynamical flow within the RNN and handling inputs arriving at arbitrary time-lags. By capturing the temporal dependencies of daily new cases, we apply it to epidemic forecasting.
- GN-ODE (Kosma et al. 2023): The method draws on recent advances in Neural ODEs to design a physics-informed neural network model that approximates the ideal SIR model in networks, thereby modeling contagion dynamics on large complex networks.
- EPINNs (Rodríguez et al. 2023): Drawing on the work of Physics-Informed Neural Networks (PINNs), EPINNs employs a dual-network structure to achieve epidemic prediction: a physics-constraints (SEIR) network learns latent epidemic dynamics, which is then combined with another neural network module capable of ingesting multiple data sources for collaborative prediction.
- EARTH (Wan et al. 2025): EARTH integrates Neural ODEs with epidemiological SIR mechanisms to learn continuous regional transmission patterns. It then utilizes a cross-attention mechanism to fuse global and local

key information, thereby providing a flexible approach to predicting epidemic spread.

E Performance Comparison

We present an additional comparison of Epi²-Net with other baselines on four real-world epidemic datasets. From Table 5, Epi²-Net continues to demonstrate superiority across all four datasets on metrics RMSE. It can be concluded that Epi²-Net achieves sota performance in epidemic dynamics modeling, as evidenced by both RMSE and MAE metrics.

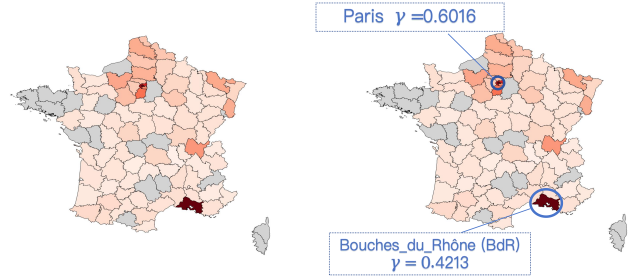


Figure 6: Visualization of the learned γ values for each region from Epi²-Net. The heatmap represents the magnitude of γ for each region in France.

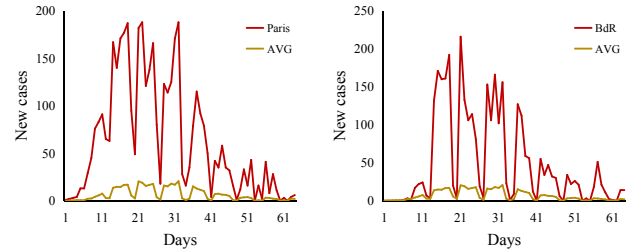


Figure 7: The infection status of two critical regions: Paris and Bouches-du-Rhône (BdR), and the French national average epidemic situation.

F Case Study

In addition to the case presented in the main text, we demonstrate Epi²-Net’s excellent performance and interpretability for real-world epidemic forecasting via more case analysis in this section.

Model interpretability. Given that the learnable reaction term coefficient γ , within the proposed neural epidemic transport equation, reflects, to a certain extent, a region’s infection trend, we visualize the γ values learned by Epi²-Net for different regions in France in Figure 6. Observing the visualization results, it is clear that the γ values of two regions are significantly higher than the average level. Upon verification, these two regions are identified as Paris and Bouches-du-Rhône (BdR), with their corresponding γ being 0.6016 and 0.4213, respectively. Consequently, we visualized the infection status of these two regions alongside

Table 5: The overall performance comparison of epidemic dynamics forecasting on metric RMSE. The bold and underlined fonts show the best and the second best result. The improvement(%) is calculated based on these two results.

Model	England			France			Italy			Spain		
	3 days	5 days	7 days	3 days	5 days	7 days	3 days	5 days	7 days	3 days	5 days	7 days
HA	9.68	10.21	10.64	11.49	11.61	11.81	48.97	48.06	47.62	135.95	136.29	136.19
PROPHET	12.67	13.58	17.73	15.79	16.60	17.12	76.96	79.83	81.81	115.44	116.89	116.58
ARIMA	9.05	9.88	9.82	11.87	11.36	11.63	79.13	68.08	65.76	108.87	109.12	109.92
LIN_REG	11.84	12.40	12.15	10.35	10.28	10.15	52.83	52.68	53.64	120.24	124.69	122.46
RAND_FOREST	10.87	10.05	10.36	6.05	5.89	5.52	48.14	49.96	49.46	65.13	67.11	62.10
XGBOOST	10.58	10.25	10.14	7.20	7.44	7.32	48.51	49.67	49.47	61.24	61.93	63.41
ITRANSFORMER	8.17	8.29	8.54	5.12	5.27	5.35	33.66	33.91	33.72	45.86	47.05	43.84
TIMEMIXER	8.05	8.12	8.23	4.83	4.95	5.13	33.62	33.79	33.99	43.86	46.25	45.77
STGNN	8.96	8.83	9.32	5.54	5.25	5.27	39.40	39.92	39.94	41.64	41.15	41.89
ATMGNN	8.09	8.14	<u>8.15</u>	5.14	5.28	<u>5.07</u>	38.39	38.95	39.56	<u>41.27</u>	40.94	40.97
ODE-LSTM	10.19	10.33	10.42	6.67	6.89	7.18	48.67	48.62	49.03	50.02	50.03	50.26
GN-ODE	11.56	11.84	11.92	9.84	9.77	10.03	45.23	45.82	45.29	52.23	51.18	55.52
EPINNs	8.82	9.31	9.42	5.56	5.52	5.50	33.23	33.45	33.52	44.92	44.68	45.08
EARTH	<u>7.97</u>	<u>8.05</u>	8.29	5.52	5.43	5.30	<u>32.54</u>	<u>32.82</u>	<u>32.19</u>	42.23	42.65	42.68
Epi ² -Net	7.57	7.78	8.08	4.73	4.77	4.52	31.61	31.00	31.28	40.41	40.77	40.05
Improvement(%)	5.01	3.35	0.85	2.07	3.63	10.84	2.85	5.54	2.82	2.08	0.41	2.24

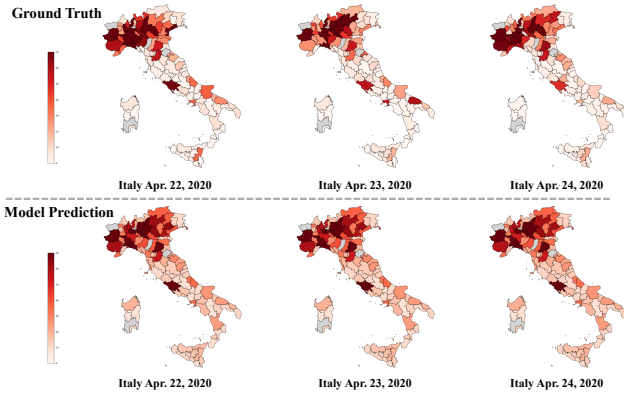


Figure 8: A case study examines COVID-19 progression in partial regions of Italy. Gray shading denotes areas lacking surveillance records.

the average infection status across all of France in Figure 7. It is evident that Paris and Bouches-du-Rhône are severely affected areas (or hotspots) by the COVID-19 epidemic in France. Considering Paris’s central geographical location and BdR’s (Bouches-du-Rhône’s) port location, the COVID-19 epidemic continued to escalate in these two places. Furthermore, the actual measures taken by the French government also corroborate our findings. As of August 2020, both regions had been designated by the French government as “highly vulnerable areas” to the COVID-19 epidemic. The preceding discussion highlights the interpretability of the Epi²-Net, suggesting that adopting intervention measures based on its predictions represents a promising approach.

Prediction performance. Here, we further elaborate on EpiNet’s predictive capabilities through more case studies. Beyond the French epidemic discussed in the main text, we

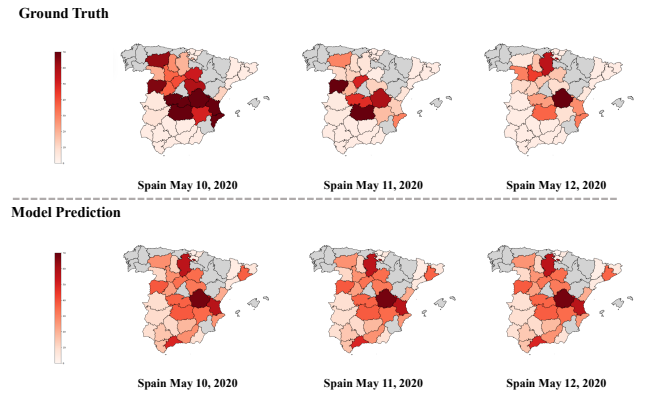


Figure 9: A case study examines COVID-19 progression in partial regions of Spain. Gray shading denotes areas lacking surveillance records.

have also visualized model’s epidemic predictions for Italy, and Spain in Figure 8 and Figure 9. What we need to emphasize is that in the epidemic forecasting task for regions in Italy, the predictions made by our model are highly consistent with the actual outcomes.

G Ablation Study

Impact of temporal encoder. Due to space limitations, we present partial ablation experiment results for the temporal encoder in the main body. Table 6 presents the complete ablation experiment results on four real-world COVID-19 datasets for the encoder. Performance comparison reveals that adopting GRU as the encoder offers advantages across all datasets. Therefore, we employ it for capturing temporal patterns within the Epi²-Net framework. Furthermore, using LSTM as an encoder can also achieve competitive per-

Table 6: Performance comparison of different temporal encoders on four real-world COVID-19 datasets. The bold and underlined font show the best and the second best result, respectively.

Encoder	England						France					
	3 days		5 days		7 days		3 days		5 days		7 days	
	RMSE	MAE										
LSTM	<u>7.68</u>	<u>5.46</u>	<u>7.86</u>	<u>5.56</u>	<u>8.12</u>	<u>6.02</u>	<u>4.91</u>	2.34	4.96	2.81	<u>4.60</u>	<u>2.66</u>
TCN	8.58	6.56	8.72	6.80	8.85	6.96	4.76	3.15	4.84	3.09	4.65	3.03
Transformer	9.32	7.63	9.48	7.83	9.67	7.97	5.27	3.24	5.34	3.22	5.12	3.18
GRU	7.57	5.35	7.78	5.50	8.08	5.70	4.73	<u>2.55</u>	4.77	2.62	4.52	2.54

Encoder	Italy						Spain					
	3 days		5 days		7 days		3 days		5 days		7 days	
	RMSE	MAE										
LSTM	<u>32.18</u>	<u>20.13</u>	34.05	21.00	34.79	21.54	47.05	37.14	47.40	36.81	47.24	36.38
TCN	33.80	20.68	<u>32.56</u>	<u>20.72</u>	33.30	21.23	53.84	38.53	54.70	38.89	54.74	38.61
Transformer	32.79	24.00	<u>32.86</u>	24.48	<u>33.62</u>	<u>25.18</u>	<u>41.41</u>	<u>33.03</u>	<u>41.77</u>	<u>34.02</u>	41.05	34.13
GRU	31.61	18.14	31.00	18.21	31.28	18.53	40.41	25.59	40.77	25.19	40.05	24.18

Table 7: Performance comparison of different decoders on four real-world COVID-19 datasets. The bold and underlined font show the best and the second best result, respectively.

Encoder	England						France					
	3 days		5 days		7 days		3 days		5 days		7 days	
	RMSE	MAE										
Linear	7.68	5.42	7.80	5.61	8.16	5.84	4.92	2.98	4.85	2.64	4.63	2.72
MLP	7.07	5.12	7.08	5.13	7.18	5.20	<u>4.79</u>	<u>2.96</u>	4.52	2.84	4.14	2.70
Non-neural	<u>7.57</u>	<u>5.35</u>	<u>7.78</u>	<u>5.50</u>	8.08	5.70	4.73	2.55	<u>4.77</u>	<u>2.62</u>	<u>4.52</u>	<u>2.54</u>

Encoder	Italy						Spain					
	3 days		5 days		7 days		3 days		5 days		7 days	
	RMSE	MAE										
Linear	<u>32.29</u>	18.84	<u>31.40</u>	<u>18.17</u>	<u>31.98</u>	<u>18.72</u>	48.20	43.78	48.54	43.73	48.74	43.94
MLP	33.73	22.67	<u>33.28</u>	<u>22.95</u>	33.81	23.41	<u>44.07</u>	<u>38.51</u>	44.56	38.84	44.14	38.63
Non-neural	31.61	18.14	31.00	18.21	31.28	18.53	40.41	25.59	40.77	25.19	40.05	24.18

formance, while TCN as an encoder performs poorly. Surprisingly, the advanced Transformer architecture performed poorly in our scenario. We infer that this might be because our observation window length for encoder is not long (default set to 7), so the Transformer’s powerful long-range modeling capabilities cannot be well demonstrated.

Impact of decoder. In our implementation, we refer to (Ji et al. 2022; Hettige et al. 2024) and adopt a parameter-free decoder to generate epidemic dynamics predictions. To study the efficacy of the decoder, we compare our model with these variants: 1) Linear: adopt a linear layer as the decoder 2) MLP: adopt a two layer-MLP as the decoder 3) Non-neural: adopt reshaping and aggregation steps to produce the desired output format. Table 7 presents the complete ablation experiment results on four real-world COVID-19 datasets for the decoder. According to the results, We can observe that using a non-neural decoder achieved ex-

cellent performance in most cases; the MLP decoder performed superiorly on the England and France datasets but poorly on the Italy dataset; the Linear decoder performed slightly worse compared to the MLP and non-neural decoders. Therefore, we recommend using a parameter-free operation to implement the decoder in Epi²-Net, due to its excellent and relatively stable performance.

H Model Stability

Numerical stability. Here, we present the numerical stability experiments of Epi²-Net. Due to its intricate architecture, which integrates modules including a Neural ODE Module, a temporal encoder, learnable coefficients, and a fully-connected layer, Epi²-Net’s numerical stability requires verification. Figures 10 illustrate Epi-Net’s training loss curves on four datasets. From these, it is evident that Epi-Net’s loss rapidly declines and converges during training, thereby showcasing the numerical stability of its model.

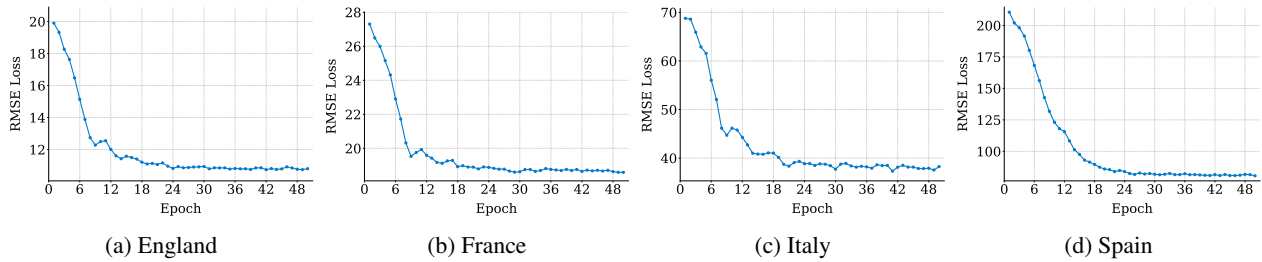


Figure 10: Numerical stability experiments of Epi²-Net on four real-world COVID-19 datasets.

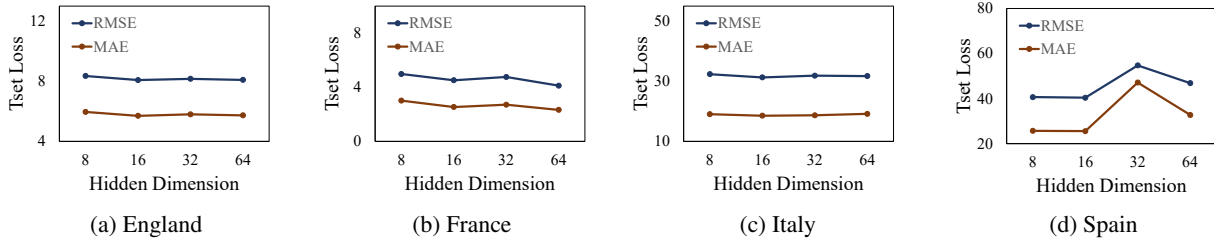


Figure 11: Hyperparameter sensitivity analysis of hidden dimension for the GRU encoder in the Epi²-Net.

Hidden dimension of encoder. To assess Epi²-Net’s robustness to hyperparameter selection, we performed a sensitivity analysis on the hidden dimension of the GRU encoder. As shown in Figure 11, the hidden dimension exhibits low sensitivity across the four real-world COVID-19 datasets, consistently achieving good performance.

I Discussions

In the main text, we briefly summarized the limitations of the Epi²-Net; in this section, we will delve deeper into its potential limitations in real-world scenarios. Furthermore, by discussing the limitations of this paper, we also hope to inspire thought within the epidemic modeling community and contribute some promising research directions to advance AI-enabled public health.

Complexity for real-world epidemic. The current framework models real-world epidemic dynamics based on physical transport, novelly integrating diffusion, convection, and reaction processes with the geographical spread of the epidemic, human mobility-driven dissemination, and regional dynamics. It effectively reconciles neural representations with physical prior knowledge. However, real-world epidemic scenarios involve more complex factors, such as population vaccination rates, public relapse and hospitalization rates, drug resistance, and the probability of viral mutation. Therefore, how to incorporate these factors is both a limitation of the framework proposed in this paper and a question worth considering for future research.

Data resources and model architecture. In addition to the various numerical data mentioned above, we also need to consider how to extend the current framework to utilize cross-modal data such as text-based policy announcements, genomic data of new variant strains, and epidemic rumors on

social networks to aid epidemic modeling presents a promising direction for future research (Du et al. 2024). Perhaps utilizing more advanced architectures (e.g., Transformers or Large Language Models) is a feasible solution, but how to bridge the mismatch between physic-inspired models and advanced deep learning models remains a question worth considering (Tian et al. 2024). In our framework, adopting advanced architectures like Transformer as module (see in Appendix F) shows a performance decline; fully unleashing the potential of advanced architectures is a promising research direction (Gong et al. 2025). However, the prerequisite for all of the above is how to obtain diverse and high-quality datasets in the field of public health. We call on the community to collectively build pioneering and sophisticated benchmarks to promote the domain development.

Emergent epidemic outbreak. While the forecasting results of Epi²-Net are promising, predicting emergent epidemic outbreak remains a significant challenge for epidemic modeling. Intuitively, the emergent outbreak of an epidemic refers to a rapid increase in the number of infected individuals within a short period, even affecting associated areas. Predicting such emergent outbreaks is crucial, as timely public health interventions can prevent hospital bed shortages, medical resource depletion, and even social panic. However, the concept for the task of predicting sudden epidemic outbreaks remains vague, urgently requiring a clear definition and the customization of corresponding models.

Domain generalizations. The currently proposed Epi²-Net is a domain-specific model for epidemic dynamics modeling. Considering the strong generalization of the diffusion-convection-reaction equation in fields such as atmospheric motion, ocean science, and traffic prediction, it is worth considering modifying the model for specific scenarios to equip it with powerful domain generalization capabilities.